Ann. Geophys., 30, 1297–1307, 2012
www.ann-geophys.net/30/1297/2012/
doi:10.5194/angeo-30-1297-2012

Annales Geophysicae

Intensification of dayside diffuse auroral precipitation: contribution of dayside Whistler-mode chorus waves in realistic magnetic fields

R. Shi[1,2], D. Han[1], B. Ni[3], Z.-J. Hu[1], C. Zhou[4], and X. Gu[5]

[1]SOA Key Laboratory for Polar Science, Polar Research Institute of China, Shanghai, China
[2]Department of Earth and Planetary Sciences, Kyushu University, Fukuoka, Japan
[3]Department of Atmospheric and Oceanic Sciences, UCLA, Los Angeles, CA, USA
[4]Department of Space Physics, School of Electronic Information, Wuhan University, Wuhan, Hubei, China
[5]Institute of Geophysics and Planetary Physics, UCLA, Los Angeles, CA, USA

Correspondence to: R. Shi (shirun0317@gmail.com)

Received: 25 February 2012 – Revised: 27 June 2012 – Accepted: 6 August 2012 – Published: 3 September 2012

Abstract. Compared to the recently improved understanding of nightside diffuse aurora, the mechanism(s) responsible for dayside diffuse aurora remains poorly understood. While dayside chorus has been thought as a potential major contributor to dayside diffuse auroral precipitation, quantitative analyses of the role of chorus wave scattering have not been carefully performed. In this study we investigate a dayside diffuse auroral intensification event observed by the Chinese Arctic Yellow River Station (YRS) all-sky imagers (ASI) on 7 January 2005 and capture a substantial increase in diffuse auroral intensity at the 557.7 nm wavelength that occurred over almost the entire ASI field-of-view near 09:24 UT, i.e., ∼12:24 MLT. Computation of bounce-averaged resonant scattering rates by dayside chorus emissions using realistic magnetic field models demonstrates that dayside chorus scattering can produce intense precipitation losses of plasma sheet electrons on timescales of hours (even approaching the strong diffusion limit) over a broad range of both energy and pitch angle, specifically, from ∼1 keV to 50 keV with equatorial pitch angles from the loss cone to up to ∼85° depending on electron energy. Subsequent estimate of loss cone filling index indicates that the loss cone can be substantially filled, due to dayside chorus driven pitch angle scattering, at a rate of ≥0.8 for electrons from ∼500 eV to 50 keV that exactly covers the precipitating electrons for the excitation of green-line diffuse aurora. Estimate of electron precipitation flux at different energy levels, based on loss cone filling index profile and typical dayside electron distribution observed by THEMIS spacecraft under similar conditions, gives a total precipitation electron energy flux of the order of 0.1 erg cm^{-2} s^{-1} with ∼1 keV characteristic energy (especially when using T01s), which can be very likely to cause intense green-line diffuse aurora activity on the dayside. Therefore, dayside chorus scattering in the realistic magnetic field can greatly contribute to the YRS ASI observed intensification of dayside green-line aurora. Besides wave induced scattering and changes in the ambient magnetic field, variations in associated electron flux can also contribute to enhanced diffuse aurora emissions, the possibility of which we cannot exactly rule out due to lack of simultaneous observations of magnetospheric particles. Since the geomagnetic activity level was rather low during the period of interest, it is reasonable to infer that changes in the associated electron flux in the magnetosphere should be small, and consequently its contribution to the observed enhanced diffuse auroral activity should be small as well. Our results support the scenario that dayside chorus could play a major role in the production of dayside diffuse aurora, and also demonstrate that changes in magnetospheric magnetic field should be considered to reasonably interpret observations of dayside diffuse aurora.

Keywords. Magnetospheric physics (Auroral phenomena)

1 Introduction

As a weak belt of emissions extending around the entire auroral oval but an essential linkage for the magnetosphere-ionosphere coupling, the diffuse aurora extends over a broad latitude range of 5° to 10°, mapping along field lines from

the outer radiation belts ($L \sim 4$) to the entire central plasma sheet with precipitation boundaries and peak location showing strong dependence on solar wind conditions. Based upon over-two-year POLAR/PIXIE observations which provided X ray emissions from the ionosphere primarily as bremsstrahlung from 2–12 keV magnetospheric electron precipitation, Petrinic et al. (1999) found that the average X ray auroral emissions maximize at local midnight with a secondary peak at approximately 06:00 MLT. A recent auroral precipitation study by Newell et al. (2009), developed using 11 years of particle data from the DMSP series satellites, also showed that the diffuse aurora is more intense post-midnight and into the morning hours and often relatively insignificant from post-noon through dusk, owing to the predominant eastward transport of electrons as a result of a combination of $\boldsymbol{E} \times \boldsymbol{B}$ and gradient drifting from the nightside plasma sheet. In contrast, Hu et al. (2009, 2012), using the ground-based all-sky imager (ASI) measurements at the Chinese Yellow River Station in Ny-Ålesund, Svalbard, surveyed the synoptic distribution of dayside aurora emissions and their potential correlation with the interplanetary magnetic field (IMF), indicating a pre-noon (07:30–09:30 MLT) "warm spot" characterized uniquely by an increase of 557.7 nm emissions, which is contributed by the emissions of the discrete and diffuse aurora, and a midday (09:30–13:00 MLT) gap of relatively weak green line emissions for the discrete and diffuse aurora. Miyoshi et al. (2010) proposed a model for the energy dispersion of electron precipitation associated with pulsating auroras; the dynamic structure embedded the diffuse aurora, and conducted a time-of-flight (TOF) analysis of precipitating electrons observed by the REIMEI satellite which suggested that the modulation region of wave-induced pitch angle scattering is near the magnetic equator. TOF analysis using REIMEI was also implemented by Nishiyama et al. (2011) to investigate the source region and its characteristic of pulsating aurora. Based on THEMIS electron measurements, Kurita et al. (2011) explored the transport and loss of the inner plasma sheet electrons, demonstrating that the large-scale convection electric field controls the electron transport to the inner magnetosphere and that the loss of plasma sheet electrons in the morning sector could be mainly induced by chorus-driven pitch angle scattering.

Recent comprehensive theoretical and modeling studies in combination with CRRES observations (Thorne et al., 2010; Ni et al., 2011a, b) have revealed that scattering by electromagnetic whistler-mode chorus waves is the dominant cause of the most intense diffuse auroral precipitation on the night-to-dawn side in the inner magnetosphere ($L <\sim 8$). As an important compliment to the above researches, Ni et al. (2012) proposed that electrostatic electron cyclotron harmonic (ECH) waves can be an important or even dominant driver of diffuse auroral precipitation in the nightside outer magnetosphere, through a detailed case investigation upon a coordinated postmidnight conjunction between the space-borne THEMIS EFI emission measurements and the ground-based NORSTAR MPI diffuse aurora observations near $L = 11.5$. Despite intensively improved understanding of the origin of nightside diffuse aurora, the mechanism(s) responsible for dayside diffuse aurora remains poorly understood.

In the present study, we show a representative event of intense dayside diffuse aurora observed by the Chinese Yellow River Station (YRS) ASI near noon LT. Since dayside chorus waves are persistent even during geomagnetically quiet conditions and show high occurrences at $L > 7$ (Li et al., 2009), we adopt a typical model of dayside chorus emissions at high L approximately corresponding to the field line of YRS location and the geomagnetic condition of the time, and perform a comprehensive evaluation of plasma sheet electron scattering rates by dayside chorus in realistic magnetic field models, which are subsequently used to compare with the strong diffusion limit and estimate the energy-dependent degree of loss cone filling. We demonstrate that resonant interactions with dayside lower-band chorus can lead to efficient resonant scattering of $\geq$500 eV to a few keV electrons (Hu et al., 2012) to substantially fill the loss cone and thus mainly contribute to the YRS ASI observed intensification of dayside green-line diffuse auroral precipitation, supporting that dayside chorus could play a major role in the production of dayside diffuse aurora.

2 Instrumentation and observations

The Chinese Arctic Yellow River Station (YRS) in Ny-Ålesund, Svalbard is located at the geographic coordinates 78.92° N, 11.93° E (not far from the North Pole) with the corrected geomagnetic latitude 76.24° and MLT $\approx$ UT + 3 h, as shown in Fig. 1. Three identical all-sky imagers (ASI), supplied with the narrow band interferential filters centered respectively at N_2^+ (^{1}NG) 427.8 nm, O (^{1}S) 557.7 nm and O (^{1}D) 630.0 nm, have been operated since November 2003. The auroras at 3 wavelengths show blue, green, and red color, which mainly correspond to the precipitating electrons with energies above a few keV, 0.5 to a few keV, and less than 500 eV, respectively (Hu et al., 2012). The ASI temporal resolution is 10 s, including 7-s exposure time and 3-s readout time. In principle, the specific location and high-quality equipment of YRS provide a unique opportunity for instantaneous and long-term nighttime auroral observations. Readers are referred to Hu et al. (2009) for the details of the YRS ASI and measurements.

Using the observations acquired from the YRS three-wavelength ASI, Hu et al. (2009) have examined the synoptic distribution of dayside aurora, and Hu et al. (2012) have furthered to explore the potential correlation between dayside auroral emissions and interplanetary magnetic field (IMF) condition. In contrast to those studies on the auroral distribution, this paper focuses on an intensification event of dayside diffuse auroral precipitation observed by the YRS ASI

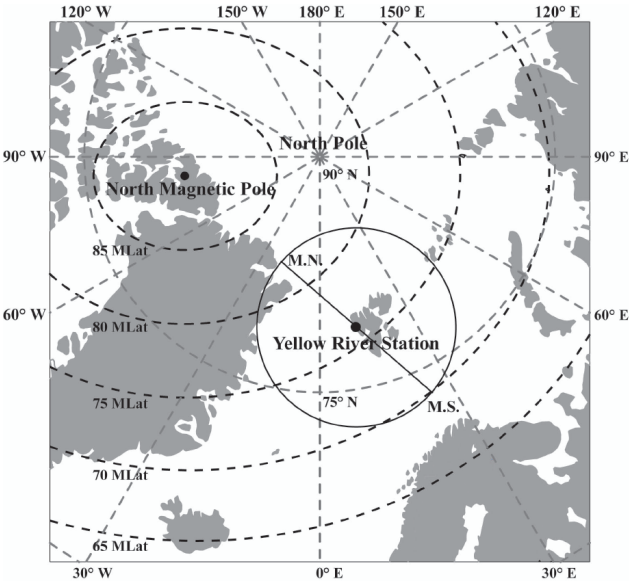

Fig. 1. The location of Yellow River Station (YRS) at geographic and geomagnetic coordinates. The solid black line circle is the field-of-view (FOV) of all-sky imagers (ASI) at YRS.

and attempts to better understand the role of resonant wave-particle scattering process and the underlying effect of chorus waves on triggering the precipitation loss of diffuse auroral electrons.

Figure 2a shows the YRS ASI observed keograms of the temporal variation of three-wavelength emission intensities along the magnetic meridian for three wavelengths, from top to bottom, at 427.8 nm, 557.7 nm and 630.0 nm, respectively, for the time interval of 07:30–10:00 UT on 7 January 2005, the corresponding solar wind parameters (including IMF B_x, B_y, B_z, solar wind speed, proton density, and dynamic pressure measured by the ACE spacecraft) and geomagnetic indices (AE and Dst) of which are illustrated in Fig. 3. The vertical axis of Fig. 2a gives the zenith angle (ZA) on the magnetic meridian (M.S. denotes magnetic south, and M.N. magnetic north), and the horizontal axis shows the universal time (UT), which has about a 3-h difference with the magnetic local time (MLT) at the YRS location. Clearly, there are strong discrete aurora emissions near 60 ZA and above, observed for both 557.7 nm and 630.0 nm wavelengths. In contrast to this, the most intense diffuse auroras occur for 557.7 nm emissions close to 09:24 UT, showing a substantial increase in diffuse auroral intensity over almost the entire ASI field-of-view. At the same time, the solar wind speed and dynamic pressure started to increase noticeably under northward IMF. While from the keogram 427.8 nm auroral emissions also increased simultaneously, they were much weaker. The later activity of diffuse aurora observed by the ASI tends to weaken somehow but becomes enhanced again near 09:42 UT. At 09:42 UT, there occurred a considerable increase in the solar wind speed and dynamic pressure and also in IMF fluctuations. Afterwards the diffuse aurora emissions turned relatively very weak, while the solar wind speed and dynamic pressure became larger. The time series of AE and Dst in Fig. 3 also show quite weak geomagnetic activity during the observed diffuse aurora intensification of our interest. Figure 2b illustrates the snap-shots of the YRS all-sky images of dayside aurora for the three wavelengths (from top to bottom: 427.8 nm, 557.7 nm, and 630.0 nm) at three specific time stamps, from left to right, 09:00:00 UT, 09:24:30 UT, and 09:48:00 UT. The magnetic meridian is given by the dashed line in each panel. At 09:00:00 UT, the auroral activity is weak for all three wavelengths, especially 427.8 nm and 557.7 nm. When it comes to 09:24:30 UT, the auroras intensify, showing the occurrence of strong discrete auroras at 427.8 nm and 630.0 nm and intense diffuse aurora at 557.7 nm. For 09:48:00 UT, there are still strong 427.8 nm and 630.0 nm discrete auroral activities, but the diffuse auroral intensity decreases considerably.

Evidently, the spatio-temporal evolution of aurora structures at different wave lengths originates from different magnetospheric causes. In contrast to the 427.8 nm emissions excited by the precipitating electrons above a few keV and the 630.0 nm emissions excited by the <500 eV soft electrons mainly from the magnetosheath (e.g., Smith and Lockwood, 1996), the 557.7 nm emissions, the focus of this study, are triggered by the atmospheric precipitation of ≥ 500 eV to a few keV electrons, which dominantly come from the magnetosphere. For plasma sheet electrons, a number of studies have demonstrated that resonant wave-particle interactions can play an essential role in driving their efficient precipitation loss (e.g., Ni et al., 2008, 2011a; Su et al., 2009; Thorne et al., 2010; Tao et al., 2011). Since moderate dayside chorus is present >10 % of the time and can persist even during periods of low geomagnetic activity (Li et al., 2009), especially at high L-shells where the YRS is located, it is natural to connect the presence of dayside chorus to the occurrence of dayside diffuse aurora.

3 Resonant scattering by dayside chorus and resultant loss cone filling

To evaluate the scattering loss effect of diffuse auroral electrons by dayside chorus, wave information including amplitude, frequency spectrum, normal angle distribution, and latitudinal spread is required to compute the quasi-linear bounce-averaged diffusion coefficients. While the conjugate wave observations in the magnetosphere is unavailable for this diffuse aurora event of our interest, there have been a number of recent studies (e.g., Li et al., 2009, 2011a; Agapitov et al., 2011) that provide considerably improved statistical global distribution of chorus, based upon long-term spacecraft measurements. In this study, we adopt the following representative parameters for dayside chorus at high L-shells ($L \sim 9.5$ for the YRS location), according to the

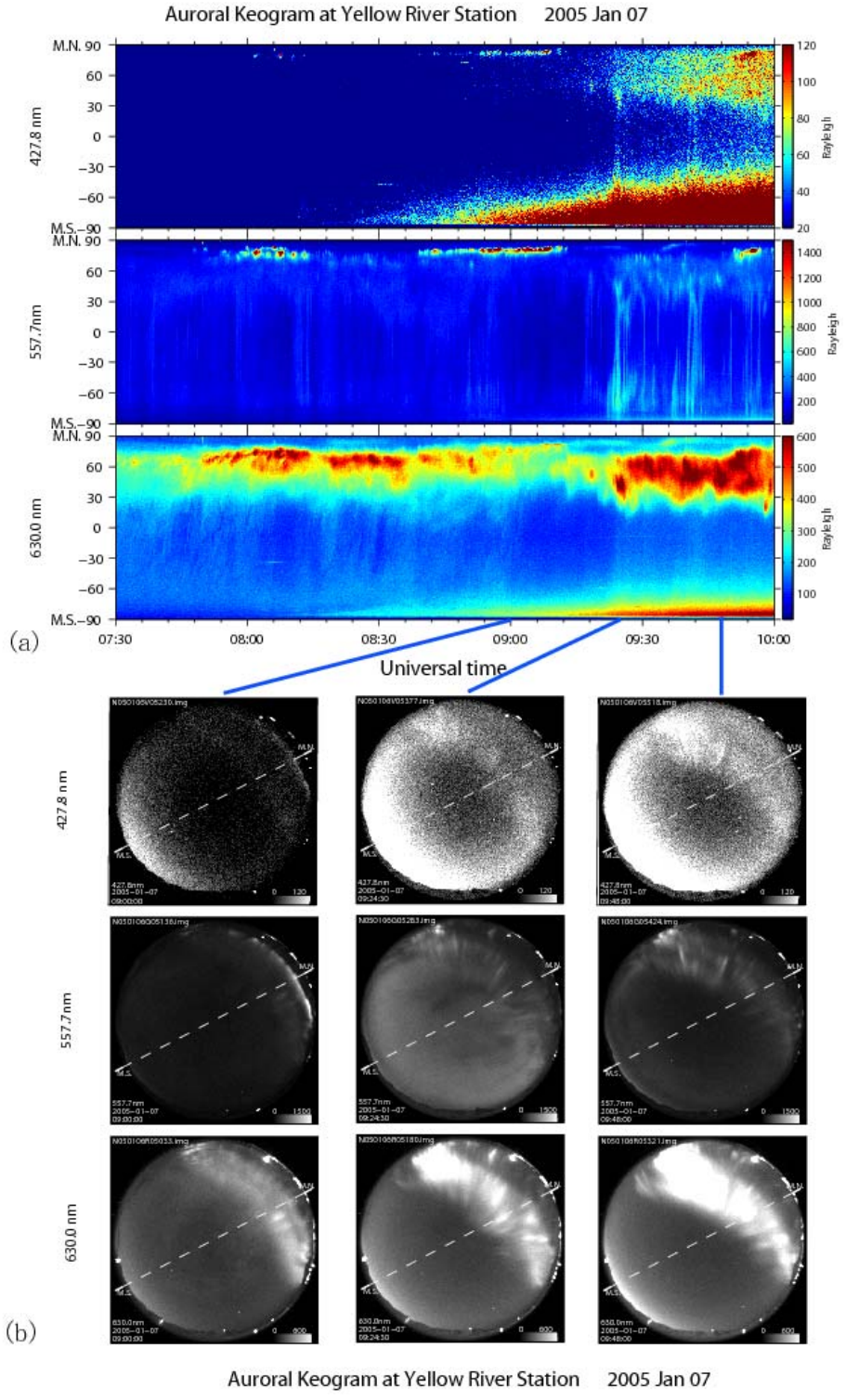

Fig. 2. (a) The YRS ASI observed keograms of the temporal variation of three-wavelength emission intensities along the magnetic meridian for three wavelengths at 427.8 nm, 557.7 nm and 630.0 nm respectively, for the time interval of 07:30–10:00 UT on 7 January 2005. The vertical axis gives the zenith angle (ZA) on the magnetic meridian (M.S. denotes magnetic south, and M.N. magnetic north), and the horizontal axis shows the universal time (UT). **(b)** The snap-shots of the YRS all-sky images of dayside aurora for the three wavelengths at 427.8 nm, 557.7 nm, and 630.0 nm at three specific time stamps, 09:00:00 UT, 09:24:30 UT, and 09:48:00 UT. The magnetic meridian is given by the dashed line in each panel. The rather uniform intensification in the southern horizon at the time interval after ∼08:30 UT is probably the dawn light.

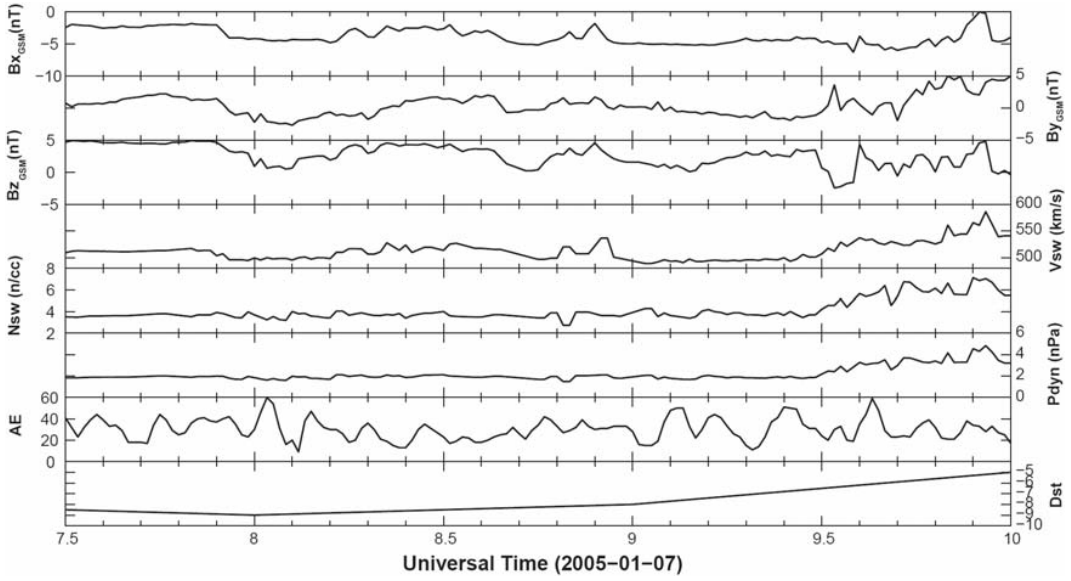

Fig. 3. Time series of solar wind parameters (including IMF B_x, B_y, B_z, solar wind speed, proton density, and dynamic pressure) and geomagnetic indices (AE and Dst) corresponding to Fig. 2a. The plotted time has been adjusted by considering the solar wind speed and the propagation time from the spacecraft to the magnetosphere.

THEMIS observations under moderate geomagnetic conditions (Li et al., 2009, 2011a): (1) the average dayside chorus wave amplitude is set as 20 pT; (2) the dayside chorus spectrum is assumed to be Gaussian with respect to wave frequency normalized to equatorial electron gyrofrequency f_{ce}, with the lower cutoff at $f_{lc}/f_{ce} = 0.1$, the upper cutoff at $f_{uc}/f_{ce} = 0.4$, the peak frequency at $f_m/f_{ce} = 0.25$, and the width of $\delta f/f_{ce} = 0.1$; (3) the wave normal angle distribution is assumed to be Gaussian over the tangent of normal angle, with the angles ranging from 0° to 45° and peaking at 0° with an angular width of 30° (e.g., Horne et al., 2005); and (4) the waves are present within 45° of the magnetic equator and are assumed as latitudinally constant.

In order to compute the scattering rates corresponding to the YRS location, we also set a latitudinally constant electron number density model with the density as $0.8\,\mathrm{cm}^{-3}$, based on satellite observations (Li et al., 2010). Following Orlova and Shprits (2010) and Ni et al. (2011c), we adopt the Tsyganenko magnetic field models rather than the dipole model to construct the more realistic configuration and field strength along the traced magnetic field line projected at the YRS location, so that the important effect of dayside magnetic field compression can be included. For the time stamp 09:24:30 UT of our interest, Fig. 4 shows the model results of field line configuration (left) in the GSM XZ plane and the magnetic field amplitude along the field line (right) corresponding to the YRS location, color-coded for different magnetic field models. Compared to the dipole field (black dashed), the field line is distorted and the profile of field amplitude exhibits considerable compression. In contrast, T89 model outputs the most stretched magnetic field configuration, and the other four Tsyganenko models present similar results that show the compression of ambient magnetic field and the double-B_{min} (magnetic field amplitude minimum) structure, implying that the latter four models tend to represent the background magnetic field distribution in a more realistic manner for the event we study. It is worth noting that double-B_{min} profiles are generated at off-equator regions by solar wind dynamic pressure and resonant wave-particle interactions have the possibility to occur at these off-equatorial regions.

We follow the following equation (Ni et al., 2011c) to quantify quasi-linear bounce-averaged pitch angle diffusion coefficients $\langle D_{\alpha\alpha}\rangle$ in non-dipolar fields,

$$\langle D_{\alpha\alpha}\rangle = \frac{\int_{\lambda_{m,s}}^{\lambda_{m,n}} \frac{D_{\alpha\alpha}(\alpha)}{\cos\alpha}\left(\frac{\tan\alpha_{eq}}{\tan\alpha}\right)^2 \sqrt{r^2+\left(\frac{\partial r}{\partial\lambda}\right)^2}\,d\lambda}{\int_{\lambda_{m,s}}^{\lambda_{m,n}} \sec\alpha\sqrt{r^2+\left(\frac{\partial r}{\partial\lambda}\right)^2}\,d\lambda}, \quad (1)$$

where $D_{\alpha\alpha}$ is the local pitch angle diffusion rate, α is the local pitch angle and α_{eq} the equatorial pitch angle, r is the radial distance to the Earth's center, λ is the magnetic latitude, and $\lambda_{m,s}$ and $\lambda_{m,n}$ are the mirror latitude of particles on the Southern and Northern Hemisphere, respectively. Our calculations include contributions from -5 to 5 cyclotron harmonic resonances and the Landau resonance. Figure 5 illustrates $\langle D_{\alpha\alpha}\rangle$ due to dayside chorus as a function of equatorial pitch-angle α_{eq} for plasma sheet electrons at nine representative energies from 100 eV to 50 keV, corresponding to the five Tsyganenko models (color coded with cyan for T89, red for T96, blue for T01, green for T01s, and black for T04s). There are a number of interesting and important features to

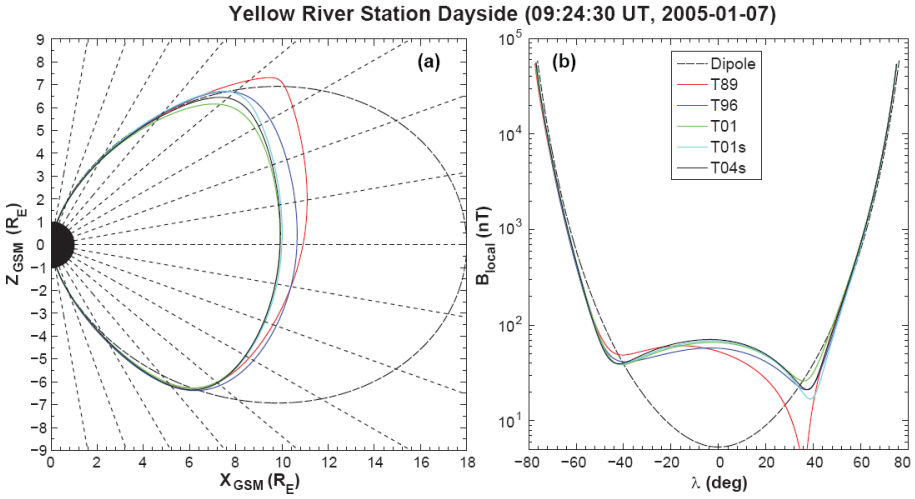

Fig. 4. (a) Modeled magnetic field configuration and **(b)** magnetic field amplitude along the field line corresponding to the YRS location for the event at 09:24:30 UT on 7 January 2005, color coded for the six specified magnetic field models.

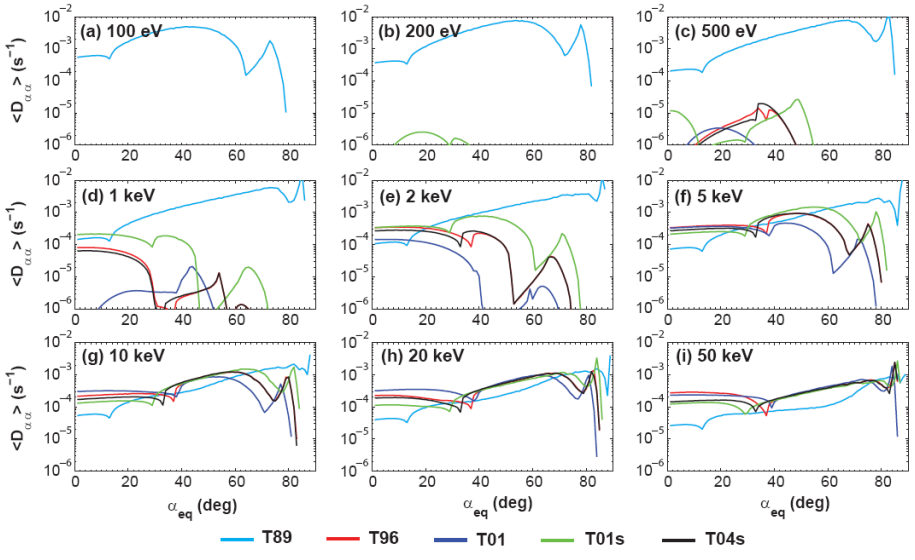

Fig. 5. Bounce-averaged pitch angle scattering coefficients $\langle D_{\alpha\alpha} \rangle$ as a function of equatorial pitch angle α_{eq} for plasma sheet electrons at the nine specified energies from 100 eV to 50 keV due to dayside chorus waves corresponding to the YRS location.

address regarding dayside chorus driven resonant scattering of plasma sheet electrons:

1. The bounce-averaged pitch angle scattering rates depend strongly on the adoption of magnetic field model. While use of T89 model can result in intense scattering of 100–500 eV electrons mainly due to modeled much lower ambient magnetic field amplitude at the equatorial region, the scattering rate results can be less trustworthy since T89 tends to represent the background magnetic field with less accuracy, compared to the other four Tsyganenko models. The differences in scattering rates between Tsyganenko models comply with the differences in modeled background magnetic field distribution.

2. The scattering effect of dayside chorus is energy dependent, most intense for $\geq\sim 1$ keV electrons and less efficient for lower energy electrons. Resonant scattering occurs at low and intermediate equatorial pitch angles for $<\sim 2$ keV electrons but can extend to higher α_{eq} close to 90° as electron energy increases.

3. The electron loss timescale due to dayside chorus scattering, estimated as the inverse of $\langle D_{\alpha\alpha} \rangle$ near the equatorial loss cone ($\alpha_{LC} \sim 1.1°$ for the event) (e.g., Shprits et al., 2006; Summers et al., 2007a, b; Summers and Ni,

Table 1. Strong diffusion rates for plasma sheet electrons at nine specified energies using different Tsyganenko magnetic field models.

	D_{SD} (s^{-1})								
	0.1	0.2	0.5	1	2	5	10	20	50 (keV)
T89	1.6e−6	2.2e−6	3.5e−6	5.0e−6	7.0e−6	1.1e−5	1.6e−5	2.2e−5	3.3e−5
T96	1.0e−5	1.4e−5	2.3e−5	3.2e−5	4.6e−5	7.2e−5	1.0e−4	1.4e−4	2.1e−4
T01	1.3e−5	1.9e−5	3.0e−5	4.2e−5	6.0e−5	9.4e−5	1.3e−4	1.8e−4	2.8e−4
T01s	8.4e−6	1.2e−5	1.9e−5	2.6e−5	3.7e−5	5.9e−5	8.3e−5	1.2e−4	1.8e−4
T04s	1.1e−5	1.5e−5	2.4e−5	3.4e−5	4.7e−5	7.5e−5	1.0e−4	1.5e−4	2.2e−4

2008), varies from tens of days for 200 eV electrons to ∼1 day for 500 eV electrons and to hours or less for ≥1 keV electrons.

Availability of quasi-linear diffusion rates enables us to quantitatively compare them with strong diffusion rate to identify energies of plasma sheet electrons that undergo strong diffusion, quasi-strong diffusion, or weak diffusion. Chen and Schulz (2001a, b) have found numerically that scattering below strong diffusion is required to better model the observed precipitating electron energy fluxes near dawn and in the morning quadrant. We evaluate the strong diffusion rate D_{SD} by

$$D_{SD} = 2(\alpha_{LC})^2/\tau_B \quad (2)$$

with bounce period τ_B and equatorial loss cone α_{LC} computed in realistic magnetic fields. The results of D_{SD} are tabulated in Table 1 for comparison with $\langle D_{\alpha\alpha}\rangle$ by dayside chorus. Clearly, as electron energy increases from 100 eV to 50 keV, the timescale of strong diffusion decreases from ∼ one day to less than one hour. Excluding the results obtained using T89 which is not reliable for this event, we can see that $\langle D_{\alpha\alpha}\rangle$ near α_{LC} exceeds or becomes comparable to D_{SD} for electrons ≥1 keV regardless of adopted magnetic field models. This suggests the approach of dayside chorus scattering to the strong diffusion limit and fully or partially filled loss cones for these relatively high energy plasma sheet electrons to largely contribute to the observed precipitation loss to the atmosphere.

Quantitative comparisons of D_{SD} with $\langle D_{\alpha\alpha}\rangle$ near α_{LC} can help us further evaluate the extent and the energy dependence of loss cone filling by dayside chorus pitch angle scattering. By defining

$$Z_0 = \sqrt{D_{SD}/\langle D_{\alpha\alpha}\rangle|_{LC}}, \quad (3)$$

an energy-dependent parameter defining the diffusion strength near the loss cone, we can compute the loss cone filling index (x) following Ni et al. (2012)

$$x(E_k) = \frac{2\int_0^1 I_0[Z_0(E_k)\tau]\cdot\tau\cdot d\tau}{I_0[Z_0(E_k)]}, \quad (4)$$

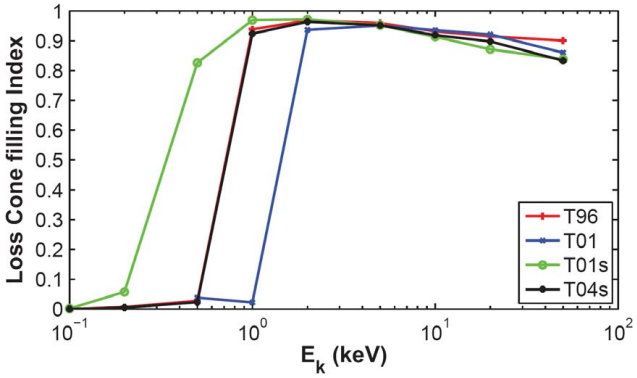

Fig. 6. Estimated loss cone filling index, based on Eq. (4), for the nine energies (100 eV, 200 eV, 500 eV, 1 keV, 2 keV, 5 keV, 10 keV, 20 keV, and 50 keV) of plasma sheet electrons, corresponding to use of color-coded Tsyganenko models.

where I_0 is the modified Bessel function of the first kind. Clearly, x is energy dependent in association with the efficiency of dayside chorus pitch angle scattering. Estimates of loss cone filling index for the diffuse auroral intensification event under consideration are shown in Fig. 6 for the nine energies of plasma sheet electrons, corresponding to use of color-coded Tsyganenko models. Obviously, there are two distinct portions of electron populations that undergo different pitch angle scattering loss into the loss cone: (1) <∼ 200 eV electrons that have empty or nearly empty loss cone distribution, and (2) >∼ 500 eV electrons that have substantially filled loss cone distribution with a filling index well above 0.8. The efficient precipitation of the latter portion due to dayside chorus pitch angle scattering is favorably consistent with the YRS ASI observed green-line diffuse auroral intensification that originated from the enhanced precipitation loss of 0.5 to a few keV plasma sheet electrons. In addition, while Fig. 6 also shows that the loss cone filling index is high in the electron energy range from a few keV to 10s keV, suggesting that ∼10 keV electrons be efficiently precipitated by dayside chorus wave scattering and potentially produce N_2^+ 427.8 nm auroral emissions, the lack of these higher energy electrons in the dayside plasma sheet during the considered geomagnetically quiet period actually accounted for the weaker activity of 427.8 nm blue-line aurora compared to

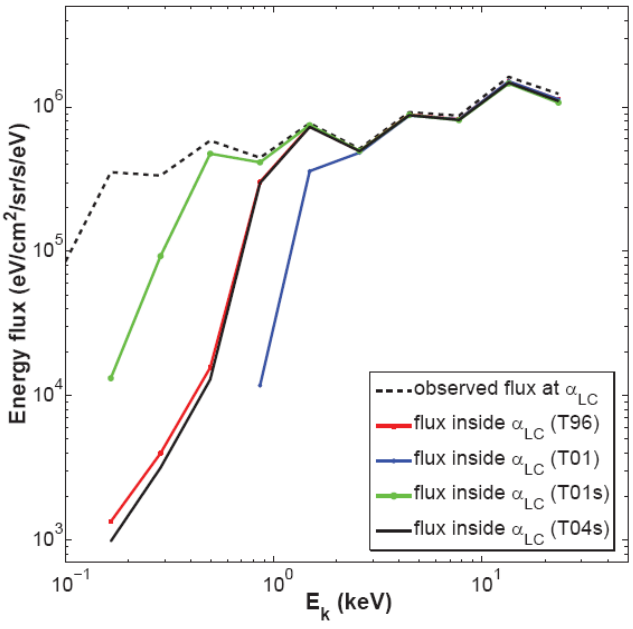

Fig. 7. Estimate of precipitation electron energy flux inside the loss cone as a function of kinetic energy color-coded for use of different Tsyganenko magnetic field models, based on the loss cone filling index profiles and a typical dayside electron distribution around the loss cone observed by the THEMIS ESA instrument at $L = 9.5$ under a similar low geomagnetic condition (dotted curve).

the simultaneously occurred 557.7 green-line diffuse auroral emissions.

Based on loss cone filling index computation and electron distribution observation, we can estimate electron precipitation flux at different energy levels, which will allow further comparisons with auroral observations. To pursue this, we have chosen a typical electron pitch angle distribution observed by THEMIS on the dayside corresponding to the similar geomagnetic condition and geomagnetic field line of YRS location, i.e., an observation of electron energy flux at $L = 9.5$ around 13:00 MLT observed by THEMIS ESA instrument on 1 September 2009 under a geomagnetically quiet condition (the dotted curve in Fig. 7). Using the calculated loss cone filling index profile, we have estimated the energy spectrum of electron distribution inside the loss cone ($<\sim 1.1^\circ$ for this case) for precipitation, the results of which are shown in Fig. 7. The color-coded curves show the precipitation electron energy fluxes resulting from dayside chorus wave scattering in T96, T01, T01s, and T04s magnetic fields, respectively. It is clear that use of T01s for chorus-induced electron scattering produces the largest precipitation electron flux, then use of T96 and T04s, and use of T01 gives the weakest precipitation flux due to the smallest degree of loss cone filling. Following the approach by Steele and McEwen (1990) and Liang et al. (2011), we have further performed a Maxwellian-type fitting to the precipitation electron differential number flux to roughly estimate the total energy flux and characteristic energy of precipitating electrons. We have obtained a total precipitation electron energy flux of $\sim$0.08 erg cm^{-2} s^{-1} with a characteristic energy of $\sim$1.9 keV for use of T01, a total precipitation electron energy flux of $\sim$0.15 erg cm^{-2} s^{-1} with a characteristic energy of $\sim$1 keV for use of T96 and T04s, and a total precipitation electron energy flux of $\sim$0.6 erg cm^{-2} s^{-1} with a characteristic energy of $\sim$800 eV for use of T01s. Although it is difficult for us to connect the estimated total precipitation energy flux with the intensity of green-line auroral emissions for straightforward comparisons, it is quite reasonable that a total precipitation electron energy flux of the order of 0.1 erg cm^{-2} s^{-1} with $\sim$1 keV characteristic energy can be very likely to cause intense green-line diffuse aurora activity on the dayside as seen in this case study.

4 Summary and discussion

We have performed a detailed investigation of the dayside diffuse auroral intensification event observed by the Chinese Arctic YRS ASI on 7 January 2005. A substantial increase in diffuse auroral intensity at the 557.7 nm wavelength has been captured to occur over almost the entire ASI field-of-view near 09:24 UT, i.e., $\sim$12:24 MLT. To check the possibility of poleward motion of the aurora, we have investigated the continuous YRS ASI observations for 09:00–10:00 UT. We captured the enhancements of green-line diffuse aurora without clear propagation effect. That is, they occurred in a sudden and covered a quite broad range of ASI FOV; there were no gradually northward moving auroral structures before their appearance; after their appearance they remained there for a while together with some expansion to other FOV space. Based on these 10-s resolution ASI observations, the observed intensification of diffuse aurora was a localized phenomenon, not a propagation effect associated with the poleward motion of the aurora.

In principle, the intensification of YRS observed green-line diffuse auroral precipitation is related to the variations of solar wind parameters manifested by fluctuations in the three components of interplanetary magnetic field (IMF) and noticeable increases in solar wind proton density and solar wind dynamic pressure. We have primarily focused on two time stamps of our interest, 09:24:30 UT and 09:42:00 UT. At 09:24:30 UT, the 557.7 nm auroral intensification occurred not with a peak value of solar wind dynamic pressure but around the start time of dynamic pressure increase from $\sim$2 nPa to $\sim$3 nPa. Corresponding to that, we can see a minor decrease in solar wind speed and a quite small increase in solar wind proton density under a nearly constant northward IMF condition. This may suggest that northward IMF condition could be a favorable factor that allows more particles "leak" into the magnetosphere for wave excitation and consequently facilitates wave-induced electron precipitation. At 09:42:00 UT, along with the 557.7 nm green-line auroral

intensification we can see a noticeable dynamic pressure increase of ∼1 nPa associated with solar wind proton density increase, as well as quite fluctuating IMF B_y and B_z. Those changes are probable to induce the marginal instability and amplification of magnetospheric chorus waves especially on the dayside (e.g., Li et al., 2011b, c) to cause intensified dayside diffuse auroral emissions.

Using a statistical model of dayside chorus waves at high L-shells based upon the THEMIS survey (Li et al., 2009, 2011a), we have computed dayside chorus driven bounce-averaged pitch angle diffusion coefficients for plasma sheet electrons in realistic magnetic field models, which have not yet been reported before but are important for quantifying the role of dayside chorus in driving dayside diffuse auroral precipitation. The results have demonstrated that dayside chorus scattering can produce intense precipitation losses of plasma sheet electrons on timescales of hours (even approaching the strong diffusion limit) over a broad range of both energy and pitch angle, namely from ∼1 keV to 50 keV with α_{eq} from the loss cone to up to ∼85° depending on electron energy. Quantitative comparisons of strong diffusion rate D_{SD} with bounce-averaged pitch angle scattering rate $\langle D_{\alpha\alpha}\rangle$ near α_{LC} provide a tool to further evaluate the extent and the energy dependence of loss cone filling by dayside chorus pitch angle scattering, which shows that the loss cone can be substantially filled for $>\sim$ 500 eV electrons with a high filling index well above 0.8 to reasonably explain the YRS ASI observed green-line diffuse auroral intensification that originated from the enhanced precipitation loss of 0.5 to a few keV plasma sheet electrons. Estimate of electron precipitation flux at different energy levels, based on loss cone filling index profile and typical dayside electron distribution observed by THEMIS spacecraft under similar conditions gives a total precipitation electron energy flux of the order of 0.1 erg cm^{-2} s^{-1} with ∼1 keV characteristic energy (especially when using T01s), which can be very likely to cause intense green-line diffuse aurora activity on the dayside. In Newell (2009), the statistical results showed that from 09:30 to 13:00 UT, the corresponding electron energy flux responsible for diffuse aurora is around 0.1 erg cm^{-2} s^{-1}, which is consistent with our simulation result. Therefore, dayside chorus can greatly contribute to the observed intensification of dayside green-line diffuse auroral precipitation, supporting the scenario that dayside chorus could play a major role in the production of dayside diffuse aurora.

As far as we know, enhancements in diffuse aurora activity have to arise from increases of precipitating electron flux, which can be due to a number of possibilities: (1) increase in the associated electron flux in the magnetosphere, (2) enhanced pitch angle scattering by waves (e.g., chorus), (3) change in the magnetic field of the magnetosphere, and (4) combinations of (1), (2) and (3). Since we did not have the simultaneous, conjugate particle measurements available, we cannot exactly rule out the possibility (1). However, since the geomagnetic activity level was rather low during the period of diffuse auroral intensification, it is reasonable to infer that the change in the associated electron flux in the magnetosphere should be small, and consequently its contribution to the observed enhanced diffuse auroral activity as well. Actually, in this study we have carefully investigated the possibilities (2) and (3) for dayside diffuse auroral intensification and found that both of them are important to appropriately understand the occurrence of dayside diffuse aurora including this event. The enhanced scattering can be well related to enhanced dayside chorus wave activity, which can be further connected to variations in solar wind condition. Full understanding of dayside chorus enhancement and its correlation with magnetic field fluctuations and solar wind dynamic pressure remains unresolved as a complex. But indeed it has been proposed that dynamic pressure enhancements, IMF fluctuations, and continuous supply of source population under northward IMF can be favorable ingredients that drive the marginal instability of dayside chorus emissions (e.g., Li et al., 2011b, c). Due to the lack of simultaneous observations of magnetospheric waves and particles for this event, we cannot give a full explanation to why the diffuse aurora enhancement was transient in Fig. 2. But quite probably it arose from the variations of dayside chorus emissions which can be also transient. Figure 1 in Nishimura et al. (2010) presented a good example on this aspect regarding the correlation between transient, discrete nightside chorus emissions and pulsating aurora activity. We plan to better understand such transient variations of dayside diffuse aurora once conjugate observations from ground-based all-sky imagers and space-borne wave and particle instruments become available.

We note that lack of simultaneous, conjugate wave measurements in space for this event challenges the quality of dayside chorus wave model adopted in the present study for numerical calculations. While we have taken into account the realistic, non-dipolar magnetic field configuration, accurate evaluation of bounce-averaged wave scattering rates also depend on reliable wave information including wave amplitude, frequency spectrum, wave normal angle distribution, and latitudinal distribution, and latitudinal background plasma density. The wave power distribution over frequency, wave normal angle and magnetic latitude is a key ingredient that controls the magnitudes of wave-induced diffusion coefficients, and the latitudinal variation of cold electron density can largely modify the resonance condition, the wave dispersion relation, and the resonance region where resonances can occur. All these factors need to be carefully addressed in our following studies. However, on the one hand, the dayside chorus wave model adopted here is currently the most improved that we can approach based on the available data source; on the other hand, our results remain useful and informative to extract the important message of how dayside chorus would pitch angle scatter plasma sheet electrons and how important this scattering effect could be for dayside diffuse auroral precipitation. We also note that to fully understand the enhancement of observed diffuse auroral intensity

evaluation of electron precipitation flux based upon loss cone filling index and observations of electron differential flux can be a feasible way (Ni et al., 2012), which however requires detailed conjunction observations of plasma sheet electron pitch angle distribution and plasma wave profiles and will be a subject of our future studies with all required data available.

Acknowledgements. This work was supported by the National Natural Science Foundation of China (41004061, 41031064, 40904041, 40974083, 40974103, 40890164, 41274164), Public Science and Technology Research Funds Projects of Ocean (201005017). Thanks are also given for the financial support of the Chinese Arctic and Antarctic Administration (IC201205). We thank Wen Li for providing us the THEMIS ESA electron distribution data. We also thank the reviewers for very constructive and valuable comments and suggestions to improve the quality of this study. BN acknowledges the support by NASA grant NNX12AD12G. RS thanks the financial support by the NICT International Exchange Program.

Topical Editor R. Nakamura thanks two anonymous referees for their help in evaluating this paper.

References

Agapitov, O., Krasnoselskikh, V., Khotyaintsev, Y. V., and Rolland, G.: A statistical study of the propagation characteristics of whistler waves observed by Cluster, Geophys. Res. Lett., 38, L20103, doi:10.1029/2011GL049597, 2011.

Chen, M. W. and Schulz, M.: Simulations of storm time diffuse aurora with plasmasheet electrons in strong pitch angle diffusion, J. Geophys. Res., 106, 1873–1886, 2001a.

Chen, M. W. and Schulz, M.: Simulations of diffuse aurora with plasma sheet electrons in pitch angle diffusion less than everywhere strong, J. Geophys. Res., 106, 28949–28966, 2001b.

Horne, R. B., Thorne, R. M., Glauert, S. A., Albert, J. M., Meredith, N. P., and Anderson, R. R.: Timescale for radiation belt electron acceleration by whistler mode chorus waves, J. Geophys. Res., 110, A03225, doi:10.1029/2004JA010811, 2005.

Hu, Z.-J., Yang, H., Huang, D., Araki, T., Sato, N., Taguchi, M., Seran, E., Hu, H., Liu, R., Zhang, B., Han, D., Chen, Z., Zhang, Q., Liang, J., and Liu, S.: Synoptic distribution of dayside aurora: Multiple-wavelength all-sky observation at Yellow River Station in Ny-Ålesund, Svalbard, J. Atmos. Solar-Terr. Phys., 71, 794–804, doi:10.1016/j.jastp.2009.02.010, 2009.

Hu, Z.-J., Yang, H.-G., Han, D.-S., Huang, D.-H., Zhang, B.-C., Hu, H.-Q., and Liu, R.-Y.: Dayside auroral emissions controlled by IMF: A survey for dayside auroral excitation at 557.7 and 630.0 nm in Ny-Ålesund, Svalbard, J. Geophys. Res., 117, A02201, doi:10.1029/2011JA017188, 2012.

Kurita, S., Miyoushi, Y., Tsuchiya, F., Nishimura, Y., Hori, T., Miyashita, Y., Takada, T., Morioka, A., Angelopoulos, V., McFadden, J. P., Auster, H. U., Albert, J. M., Jordanova, V., and Misawa, H.: Transport and loss of the inner plasma sheet electrons: THEMIS observations, J. Geophys. Res., 116, A03201, doi:10.1029/2010JA015975, 2011.

Li, W., Thorne, R. M., Angelopoulos, V., Bortnik, J., Cully, C. M., Ni, B., LeContel, O., Roux, A., Auster, U., and Magnes, W.: Global distribution of whistler-mode chorus waves observed on the THEMIS spacecraft, Geophys. Res. Lett., 36, L09104, doi:10.1029/2009GL037595, 2009.

Li, W., Thorne, R. M., Nishimura, Y., Bortnik, J., Angelopoulos, V., McFadden, J. P., Larson, D. E., Bonnell, J. W., Le Contel, O., Roux, A., and Auster, U.: THEMIS analysis of observed equatorial electron distributions responsible for the chorus excitation, J. Geophys. Res., 115, A00F11, doi:10.1029/2009JA014845, 2010.

Li, W., Bortnik, J., Thorne, R. M., and Angelopoulos, V.: Global distribution of wave amplitudes and wave normal angles of chorus waves using THEMIS wave observations, J. Geophys. Res., 116, A12205, doi:10.1029/2011JA017035, 2011a.

Li, W., Bortnik, J., Thorne, R. M., Nishimura, Y., Angelopoulos, V., and Chen, L.: Modulation of whistler mode chorus waves: 2. Role of density variations, J. Geophys. Res., 116, A06206, doi:10.1029/2010JA016313, 2011b.

Li, W., Thorne, R. M., Bortnik, J., Nishimura, Y., and Angelopoulos, V.: Modulation of whistler mode chorus waves: 1. Role of compressional Pc4–5 pulsations, J. Geophys. Res., 116, A06205, doi:10.1029/2010JA016312, 2011c.

Liang, J., Ni, B., Spanswick, E., Kubyshkina, M., Donovan, E. F., Uritsky, V. M., Thorne, R. M., and Angelopoulos, V.: Fast earthward flows, electron cyclotron harmonic waves, and diffuse auroras: Conjunctive observations and a synthesized scenario, J. Geophys. Res., 116, A12220, doi:10.1029/2011JA017094, 2011.

Miyoshi, Y., Katoh, Y., Nishiyama, T., Sakanoi, T., Asamura, K., and Hirahara, M.: Time of flight analysis of pulsating aurora electrons, considering wave-particle interactions with propagating whistler mode waves, J. Geophys. Res., 115, A10312, doi:10.1029/2009JA015127, 2010.

Newell, P. T., Sotirelis, T., and Wing, S.: Diffuse, monoenergetic, and broadband aurora: The global precipitation budget, J. Geophys. Res., 114, A09207, doi:10.1029/2009JA014326, 2009.

Ni, B., Thorne, R. M., Shprits, Y. Y., and Bortnik, J.: Resonant scattering of plasma sheet electrons by whistler-mode chorus: Contribution to diffuse auroral precipitation, Geophys. Res. Lett., 35, L11106, doi:10.1029/2008GL034032, 2008.

Ni, B., Thorne, R. M., Horne, R. B., Meredith, N. P., Shprits, Y. Y., Chen, L., and Li, W.: Resonant scattering of plasma sheet electrons leading to diffuse auroral precipitation: 1. Evaluation for electrostatic electron cyclotron harmonic waves, J. Geophys. Res., 116, A04218, doi:10.1029/2010JA016232, 2011a.

Ni, B., Thorne, R. M., Meredith, N. P., Horne, R. B., and Shprits, Y. Y.: Resonant scattering of plasma sheet electrons leading to diffuse auroral precipitation: 2. Evaluation for whistler mode chorus waves, J. Geophys. Res., 116, A04219, doi:10.1029/2010JA016233, 2011b.

Ni, B., Thorne, R. M., Shprits, Y. Y., Orlova, K. G., and Meredith, N. P.: Chorus-driven resonant scattering of diffuse auroral electrons in nondipolar magnetic fields, J. Geophys. Res., 116, A06225, doi:10.1029/2011JA016453, 2011c.

Ni, B., Liang, J., Thorne, R. M., Angelopoulos, V., Horne, R. B., Kubyshkina, M., Spanswick, E., Donovan, E. F., and Lummerzheim, D.: Efficient diffuse auroral electron scattering by electrostatic electron cyclotron harmonic waves in the outer magnetosphere: A detailed case study, J. Geophys. Res., 117, A01218, doi:10.1029/2011JA017095, 2012.

Nishimura, Y., Bortnik, J., Li, W., Thorne, R. M., Lyons, L. R., Angelopoulos, V., Mende, S. B., Bonnell, J. W., Le Contel, O., Cully, C., Ergun, R., and Auster, U.:

Identifying the driver of pulsating aurora, Science, 330, 81–84, doi:10.1126/science.1193186, 2010.

Nishiyama, T., Sakanoi, T., Miyoshi, Y., Katoh, Y., Asamura, K., Okano, S., and Hirahara, M.: The source region and its characteristic of pulsating aurora based on the Reimei observations, J. Geophys. Res., 116, A03226, doi:10.1029/2010JA015507, 2011.

Orlova, K. G. and Shprits, Y. Y.: Dependence of pitch-angle scattering rates and loss timescales on the magnetic field model, Geophys. Res. Lett., 37, L05105, doi:10.1029/2009GL041639, 2010.

Petrinec, S. M., Chenette, D. L., Mobilia, J., Rinaldi, M. A., and Imhof, W. L.: Statistical X ray auroral emissions – PIXIE observations, Geophys. Res. Lett., 26, 1565–1568, 1999.

Shprits, Y. Y., Li, W., and Thorne, R. M.: Controlling effect of the pitch-angle scattering rates near the edge of the loss cone on electron lifetimes, J. Geophys. Res., 111, A12206, doi:10.1029/2006JA011758, 2006.

Smith, M. F. and Lockwood, M.: Earth's magnetospheric cusps, Rev. Geophys., 34, 233–260, doi:10.1029/96RG00893, 1996.

Steele, D. and McEwen, D.: Electron auroral excitation efficiencies and intensity ratios, J. Geophys. Res., 95, 10321–10336, doi:10.1029/JA095iA07p10321, 1990.

Su, Z., Zheng, H., and Wang, S.: Evolution of electron pitch angle distribution due to interactions with whistler-mode chorus following substorm injections, J. Geophys. Res., 114, A08202, doi:10.1029/2009JA014269, 2009.

Summers, D. and Ni, B.: Effects of latitudinal distributions of particle density and wave power on cyclotron resonant diffusion rates of radiation belt electrons, Earth Planets Space, 60, 763–771, 2008.

Summers, D., Ni, B., and Meredith, N. P.: Timescales for radiation belt electron acceleration and loss due to resonant wave-particle interactions: 1. Theory, J. Geophys. Res., 112, A04206, doi:10.1029/2006JA011801, 2007a.

Summers, D., Ni, B., and Meredith, N. P.: Timescales for radiation belt electron acceleration and loss due to resonant wave-particle interactions: 2. Evaluation for VLF chorus, ELF hiss, and electromagnetic ion cyclotron waves, J. Geophys. Res., 112, A04207, doi:10.1029/2006JA011993, 2007b.

Tao, X., Thorne, R. M., Li, W., Ni, B., Meredith, N. P., and Horne, R. B.: Evolution of electron pitch angle distributions following injection from the plasma sheet, J. Geophys. Res., 116, A04229, doi:10.1029/2010JA016245, 2011.

Thorne, R. M., Ni, B., Tao, X., Horne, R. B., and Meredith, N. P.: Scattering by chorus waves as the dominant cause of diffuse auroral precipitation, Nature, 467, 943–946, doi:10.1038/nature09467, 2010.